HHS Public Access

Author manuscript

Mol Psychiatry. Author manuscript; available in PMC 2022 August 24.

Published in final edited form as:

Mol Psychiatry. 2022 April ; 27(4): 2291–2303. doi:10.1038/s41380-022-01474-1.

COUNTERACTING EPIGENETIC MECHANISMS REGULATE THE STRUCTURAL DEVELOPMENT OF NEURONAL CIRCUITRY IN HUMAN NEURONS

Seonhye Cheon[1,2,ξ], **Allison M. Culver**[1,2,ξ], **Anna M. Bagnell**[1,2], **Foster D. Ritchie**[1,2], **Janay M. Vacharasin**[1,2], **Mykayla M. McCord**[1,2], **Carin M. Papendorp**[3], **Evelyn Chukwurah**[1,2], **Austin J. Smith**[1,2], **Mara H. Cowen**[1,2], **Trevor A. Moreland**[1,2], **Pankaj S. Ghate**[1,2], **Shannon W. Davis**[1,2], **Judy S. Liu**[3,4,5], **Sofia B. Lizarraga**[1,2,*]

[1]Department of Biological Sciences, University of South Carolina, Columbia, SC

[2]Center for Childhood Neurotherapeutics, University of South Carolina, Columbia, SC

[3]Department of Molecular Biology, Cell Biology and Biochemistry, Brown University, Providence, RI

[4]Center for Translational Neuroscience, Robert J. and Nancy D. Carney Institute for Brain Science and Brown Institute for Translational Science, Brown University, Providence, RI

[5]Department of Neurology, Rhode Island Hospital and Warren Alpert Medical School of Brown University, Providence, RI

Abstract

Autism spectrum disorders (ASD) are associated with defects in neuronal connectivity and are highly heritable. Genetic findings suggest that there is an overrepresentation of chromatin regulatory genes among the genes associated with ASD. ASH1 like histone lysine methyltransferase (ASH1L) was identified as a major risk factor for ASD. ASH1L methylates Histone H3 on Lysine 36, which is proposed to result primarily in transcriptional activation. However, how mutations in ASH1L lead to deficits in neuronal connectivity associated with ASD pathogenesis is not known. We report that ASH1L regulates neuronal morphogenesis by counteracting the catalytic activity of Polycomb Repressive complex 2 group (PRC2) in stem cell-derived human neurons. Depletion of ASH1L decreases neurite outgrowth and decreases expression of the gene encoding the neurotrophin receptor TrkB whose signaling pathway

*Corresponding author: Sofia B. Lizarraga, PhD, Lizarras@mailbox.sc.edu.

ξThese authors contributed equally to this work

AUTHOR CONTRIBUTIONS

SBL conceived, designed, and supervised the study and conducted experiments. SHC and AMC conducted the majority of the experiments. SHC, AMC and SBL conducted the majority of the analysis. AMB, and FDR conducted imaging and gene expression experiments and contributed to the analysis of those experiments. JMV and TAM contributed to gene expression experiments and analysis. MM, MHC and AJS contributed to imaging analysis. CMP & JL conducted the imaging on the Delta vision OMX microscope. EC & PG provided neurons used for some of the experiments. SBL wrote the manuscript and put together all the final figures and tables. All co-authors contributed to editing the manuscript and interpretation of the results.

CONFLICT OF INTEREST

The authors declare no conflict of interest with this work.

is linked to neuronal morphogenesis. The neuronal morphogenesis defect is overcome by inhibition of PRC2 activity, indicating that a balance between the Trithorax group protein ASH1L and PRC2 activity determines neuronal morphology. Thus, our work suggests that ASH1L may epigenetically regulate neuronal morphogenesis by modulating pathways like the BDNF-TrkB signaling pathway. Defects in neuronal morphogenesis could potentially impair the establishment of neuronal connections which could contribute to the neurodevelopmental pathogenesis associated with ASD in patients with ASH1L mutations.

INTRODUCTION

Autism spectrum disorder (ASD) affects 1 in 44 children and represents a growing public health concern worldwide. Between 50 to 75% of ASD cases are of unknown or complex genetic etiology. One potential factor contributing to the complex etiology of ASD is the disruption of epigenetic or chromatin regulatory mechanisms [1]. Epigenetic mechanisms entail the incorporation or removal of chemical modifications on histones or genomic DNA that lead to the repression or activation of genes. Mutations in epigenetic regulators, including histone and DNA methylators, have been associated with ASD [1, 2]. In particular, there is a significant over-representation of chromatin regulators (over 40%) among genes that contain high-risk variants for ASD, according to the SFARI curated database of autism genes [3]. Specifically, de novo truncating and missense mutations in the chromatin regulator *Absent, Small, Or Homeotic-Like (ASH1L)* have been identified in large ASD cohorts [4–6]. Loss of function due to haploinsufficiency in *ASH1L* but not complete loss of ASH1L protein appears to be the common determinant among the pathogenic variants [7]. Furthermore, recent evidence suggests that ASH1L is associated with severe forms of autism, as patients with mutations in ASH1L suffer from intellectual disabilities, speech difficulties, seizures, and postnatal microcephaly (failure of the brain to grow postnatally) [8–10]. Therefore, the human phenotypes associated with mutations in ASH1L suggest a major role for this chromatin modifier during the development of neuronal connectivity.

ASH1L is a member of the Trithorax group of proteins. Trithorax proteins are major regulators of embryonic development that are proposed to antagonize the activity of the Polycomb repressor complex [11]. In particular, ASH1L dimethylation on Histone H3 on Lysine 36 (H3K36me2) antagonizes the activity of the Polycomb Repressor Complex 2 (PRC2) by preventing the trimethylation of Histone H3 on Lysine 27 (H3K27me3) [12, 13]. The function of PRC2 in neuronal development has been associated with cell fate control of neurogenesis [14, 15], and more recently, has been linked to neuronal maturation, as its catalytic subunit Enhancer of Zeste Homolog 2 (EZH2) is proposed to modulate neuronal arborization [16]. In comparison to PRC2, the function of ASH1L in neuronal development is largely understudied. We report an essential role for ASH1L in neuronal morphogenesis. Using stem cell-derived human neurons [17–19], we show that acute knockdown of *ASH1L* in forebrain cortical excitatory neurons reduces neurite growth and arborization. One of the cellular mechanisms that underlie brain growth after birth is the development of neuronal arbors; therefore, failure to form connections due to reduced neuronal arborization could impair subsequent neuronal connectivity. The neuronal arborization defect in ASH1L deficient neurons correlates with enlarged phalloidin-positive

structures at the growing ends of neurites, which could be indicative of stalled axon growth or guidance defects. We propose that this regulation of neuronal growth is modulated by counteracting epigenetic mechanisms between ASH1L and PRC2, as we can rescue the ASH1L associated neuronal morphogenesis defects by inhibiting the activity of the PRC2 complex protein EZH2 [11, 20]. Furthermore, we uncover ASH1L as a novel regulator of the neurodevelopmentally important BDNF-TrkB signaling pathway, which is essential for proper neuronal arborization during development [21], as well as synapse development and function [22]. We show that the levels of *NTRK2*, the gene encoding the neurotrophin receptor TrkB, are significantly decreased in human neurons deficient for ASH1L compared to the other neurotrophin receptors. Downregulation of TrkB is sufficient to render the neurons unable to respond to exogenous BDNF, as the neuronal morphogenesis phenotypes are not rescued upon exposure to BDNF. Therefore, we propose that the deficit in TrkB expression caused by ASH1L knockdown contributes to the defects in neuronal morphogenesis. Taken together, we present evidence of ASH1L's modulation of neuronal morphogenesis by counteracting the activity of the PRC2 complex and by regulating the BDNF-TrkB signaling pathway.

MATERIALS AND METHODS

Identification of *ASH1L* positive and negative correlated genes with functional enrichment analysis

Gene expression data was obtained from the Allen Brain Atlas Developmental Transcriptome Database (© 2010 Allen Institute for Brain Science. Allen Human Brain Atlas. Available from: human.brain-map.org) [23, 24]. Transcriptome data was obtained from RNA-sequencing and exon microarray hybridization that was generated across 13 developmental stages and 8-16 brain structures. (See Supplementary methods and Supplementary Tables S1, S2 and S3). To identify genes with similar expression patterns to *ASH1L* and other genes of interest in the study, the correlative search option within the Developmental Transcriptome Database was used. This function finds genes with similar expression patterns over the entire dataset or over a subset of structures and developmental stages [23]. We focused the correlative search on structures of the prefrontal cortex (PFC) composed of the dorsolateral prefrontal cortex (DFC), ventrolateral prefrontal cortex and the mediolateral prefrontal cortex at stages 8 to 37 weeks post conception (pcw) of prenatal development. We also analyzed the DFC alone at stages 8 to 18 pcw. We identified genes with either the highest positive correlation (r) ($0.7 < r < 1$) or negative correlation ($-1 < r < -0.7$) to *ASH1L* gene expression. To analyze the function of top positive or negative correlated genes we used Toppgene software (https://toppgene.cchmc.org/enrichment.jsp) to detect functional enrichment based on Transcriptome, Proteome, Ontologies (GO, Pathway), Phenotype (human disease and mouse phenotype), and literature co-citation [25]. Genes were imported into the portal, and resulting functional enrichments were ranked by adjusted p-value (Supplementary Tables S4, S5 to S8).

Reverse Transcriptase quantitative PCR (RT-qPCR) analysis of gene expression

Total RNA was harvested using a total RNA mini or micro-isolation kits (Qiagen catalog #74104 or #74034) and was reverse transcribed to cDNA using the Superscript

reverse transcription kit (Invitrogen catalog #18080-051), following manufacturer's recommendations. Gene expression levels were determined using SYBR green with IDT designed primers (Supplementary Table S9) using a CFX96 Touch Real Time PCR Detection System (BioRad). A detailed protocol is included in the supplementary methods.

Acute knockdown of ASH1L in hESC derived human excitatory neurons

Stem cell cultures and neuronal differentiation were conducted as previously described [17, 19, 26]. Unless otherwise indicated human embryonic stem cell (hESCs) line H1 [27] was used to differentiate human cortical neurons for most of the experiments. In addition, human induced pluripotent stem cell (iPSC) line 20B [28] was also used to differentiate human cortical neurons for studies that analyzed gene expression for CREB pathway components. For extensive methods used see supplementary methods section. shRNA lentiviral constructs targeting ASH1L, containing a puromycin resistance cassette were purchased from Sigma (Supplementary Table S10). For each reaction, 400,000 human cortical neurons [17] between days 28 to 30 were nucleofected with control or ASH1L shRNAs constructs using the X-unit of the Amaxa nucleofector unit (Lonza, catalog # AAF1002X) per manufacturers protocol. Neurons were subjected to puromycin selection a day after nucleofection and were harvested 72 hours (hrs.) post puromycin treatment unless otherwise indicated. A detailed protocol is included in the supplementary methods.

Digital Droplet PCR (ddPCR) analysis of TrkB isoforms

To conduct ddPCR analysis, primers were custom designed for specific TrkB isoforms (Supplementary Table S11). Primers and probes were purchased from IDT technologies. ddPCR experiments were conducted using a QX200 Droplet Digital PCR (ddPCR™) System – Bio-Rad. A detailed protocol is included in the supplementary methods.

Immunostaining and phalloidin staining of human forebrain cortical neurons

Nucleofected human neurons were fixed and immunostained with specific antibodies or stained with phalloidin as previously described [29]. A detailed protocol and antibody information is included in the supplementary methods.

EZH2 and BDNF treatment of ASH1L knockdown neurons

To determine the capacity of exogenously added BDNF or EZH2 inhibitors to rescue the ASH1L associated neuronal phenotypes, we treated nucleofected neurons 48 hrs. after the initial puromycin treatment with either BDNF (PeproTech, Catalog #450-02) at 10ng/ml or EZH2 inhibitor EI1 (Sigma-Aldrich /Calbiochem, Catalog #5005610001) at 1.25 μM and 2.5μM. For BDNF experiments, treatments were carried out for 72 hrs. as previously described in studies with human neurons with defects in BDNF-TrkB signaling [19]. For EZH2 inhibition experiments, treatments were carried out for either 72 hrs. or 120 hrs. based on previously described studies on non-neuronal cells [30] and calculation of neuronal survival at different dosages. After the initial treatment neurons were fed with half media changes every other day containing the final concentration of either BDNF or EZH2 inhibitor (see supplementary material for experimental detail).

Image Acquisition

For neuronal arborization and growth cone studies images were taken using either a Leica DMI3000 or DM6000 widefield fluorescence microscope. For analysis of phospho-CREB signal, cells were imaged with conventional widefield microscopy with deconvolution. In GFP-expressing neurons, super resolution images of the nucleus were taken using structured illumination microscopy (DeltavisionOMX-SR). This technique was used to ascertain the distribution of Phospho-CREB in the nucleus.

Image Analysis

Neuronal arborization: To analyze neuronal arborization parameters we utilized Neurolucida 360 software and traced GFP stained neurons after confirming that they were positive for β-III-Tubulin. The tracing was conducted on the GFP channel. Observers carrying out the tracing were blinded to experimental conditions. The cell bodies were detected using the "detect all soma" button on the cell body panel. The dendrites were then traced by changing the controls to "user guided kernels", following each dendrite starting at the cell body. The complexity index (CI) measure considers changes in branch number, length, and number of primary neurites [31]. CI was calculated by Neurolucida software based on the following equation: *CI = [Sum of sister branches emanating from the dendritic segment between a particular terminal tip and cell body + Number of endings]*[Total neurite length/Total Number of primary neurites].*

Soma size: To analyze differences in cell body size, neuronal somas were manually traced using image J software in the GFP channel after confirming that the cells were positive for β-III-Tubulin.

Phalloidin positive structures: For this analysis we focused on regions at the ends of the neurites that were stained for phalloidin. To quantify the size of the phalloidin positive structures at the growing ends of neurites, we used ImageJ software to threshold the images and draw regions of interest (ROI) around phalloidin stained areas to measure area, perimeter, and integrated density of each ROI. The number of phalloidin positive areas was counted simultaneously from the ROI.

Phospho-CREB nuclear translocation: To quantify the total content of phospho-CREB translocated to the nucleus, we used ImageJ software. 16-bit Images for DAPI and phospho-CREB were analyzed. ROIs were drawn around each nucleus in the DAPI channel and then added to the ROI manager and loaded onto the phospho-CREB channel and measured. A background area was also measured for each phospho-CREB image. Mean fluorescent intensity (MFI) was calculated using the following formula: *MFI = Integrated density of phospho-CREB – (phospho-CREB area*mean grey value background)*

Neuronal marker analysis: To determine changes in neuronal cell fate overlay images were analyzed using the cell counter function in ImageJ. Each channel or overlapping channels were assigned to a specific counter category.

Statistical Analysis

Unless otherwise specified, all data was analyzed using GraphPad statistical analysis software and multiple groups were either analyzed using one-way ANOVA with multiple comparisons without correction when compared to a single control or using a two-way ANOVA with multiple comparisons without correction for multiple comparisons when multiple treatments or conditions were compared or using paired or unpaired t-tests. A summary of statistical parameters for each experiment is found in Supplementary materials (Supplementary Table S12).

RESULTS

ASH1L is dynamically expressed during human brain development

Because *ASH1L* is linked to ASD, we sought to determine the spatiotemporal expression pattern of *ASH1L* in the developing human brain using available databases, as a determinant of whether ASH1L could contribute to neuronal connectivity. Using transcriptome data from human postmortem brain samples obtained from the Allen Brain Atlas [24], we analyzed the expression of *ASH1L* during fetal development (Fig. 1A, Supplementary Table S1 to S3 and Supplementary Methods). *ASH1L* showed the highest expression between pcw 9 to 17 in prefrontal cortical (PFC) structures, including the dorsolateral, ventrolateral, and medial prefrontal cortex (DFC, VFC, MFC). ASH1L is an epigenetic regulator that generally activates transcription [32, 33]. However, its function or the pathways that are modulated by ASH1L in neuronal development are not well understood. Therefore, we analyzed genes that are either positively or negatively correlated by expression with *ASH1L* to begin an analysis of the pathways that might be modulated by ASH1L during neuronal development. We used a correlation coefficient algorithm provided by the Allen Brain Atlas, which identifies the most highly positively or negatively correlated genes with ASH1L by co-expression analysis. This was defined by a correlation coefficient (r) greater than 0.7 for positive correlation or smaller than −0.7 for negative correlation. We conducted the analysis within the three structures of the PFC, during the entire prenatal window (8 to 37 pcw) and then more specifically the DFC during 8 to 18 pcw (Supplementary Table S4). Using the most highly positively or negatively co-related genes for either the PFC or DFC we conducted pathway analysis [25]. Analysis of the negatively correlated genes ($-1 < r < -0.7$) showed an overrepresentation of genes associated with mitochondrial function, RNA or Ribosomal biosynthesis and Mitochondrial associated diseases like Leigh syndrome [34] in the PFC and DFC (Fig. 1B, Supplementary Fig. S1 and Supplementary Table S5–S6). In contrast, analysis of positively correlated genes in the PFC showed enrichment of chromatin regulatory pathways (Fig. 1B, Supplementary Fig. S1 and Table S7), while both the DFC and PFC showed an overrepresentation of genes involved in neuronal projection development or morphogenesis, axonal or synaptic function, intellectual disability, developmental delay, and autistic behaviors (Fig. 1B, Supplementary Fig. S1 and Table S7–S8). Together, these findings, suggest a role for ASH1L in neuronal morphogenesis. We decided to further interrogate this possibility by modeling neuronal development using human stem cell derived cortical excitatory neurons (Fig. 1C) [17].

Autism has a higher incidence in males than females [35]. To date, the majority of *ASH1L* mutations have been reported in males with variable phenotypes [4, 5, 9, 10, 36, 37]. Therefore, we used male stem cells to generate human neurons. We differentiated WA01 (H1) male human embryonic stem cells (hESCs) [27] forebrain cortical excitatory neurons [17]. We analyzed ASH1L gene (Fig. 1D) and protein (Fig. 1E and Supplementary Figure S2A) expression at day 0 for stem cells, at day 12 for neuroepithelial cells, at day 21 for neuronal progenitor cells, just as neurogenesis starts in these cultures, and at day 30 when deeper layer cortical excitatory neurons arise *in vitro* (see supplementary methods). We confirmed the *in vitro* developmental stage of our cultures using the following markers: NANOG for stem cells, PAX6 for neuronal progenitors, and MAP2 for mature neurons in four independent experiments (Fig. 1D–E, Supplementary Table S9). We found that at the mRNA and protein levels ASH1L was expressed throughout the four *in vitro* developmental timepoints we analyzed (Fig. 1D–E). Taken together these findings suggest that ASH1L function is important at multiple stages of development, which correlates with the embryonic lethality of *Ash1l* $^{-/-}$ mouse embryos [38].

ASH1L regulates neuronal morphogenesis but does not alter neuronal cell fate.

A pathogenic variant in *ASH1L* has been associated with postnatal microcephaly, or failure of the brain to grow after birth [10]. Postnatal microcephaly could arise from defects in neuronal axonogenesis, axonal and dendritic arborization, or synaptogenesis [39]. A role for ASH1L in synaptic function has been described in mice [38, 40]. Homozygous null ASH1L mice are embryonic lethal [38] or die at the newborn stage [40], while the heterozygous animals reported to date do not have any obvious structural brain phenotypes [38]. Based on the pathways we identified in the correlation analysis (Fig. 1 and Supplementary Fig. S1) and the human patient phenotypes [10], we decided to test the assumption that deficits in ASH1L in humans might compromise neurite outgrowth. To address this, we first tested five different shRNA constructs for knockdown of endogenous ASH1L in HEK293T cells and identified three shRNA constructs (shRNA2, 3 and 4) that consistently gave close to 80% knockdown of ASHL1 protein after puromycin selection compared to control (Supplementary Fig. S2B–C, Supplementary Table S9 and Supplementary Methods). GFP control construct alone or ASH1L-shRNA plus a GFP construct were transfected into male cortical neurons and subjected to puromycin selection for 72 hrs. (Fig. 1F and Supplementary Fig. S2D). shRNA transfection of these cortical neurons significantly reduced ASH1L gene expression levels by an average of 65.2% (Fig. 1F), compared to control transfected neurons, with no significant differences between the different ASH1L shRNA transfected neurons. In published mouse models of ASH1L deficiency, the reduction in ASH1L levels in heterozygous animals is between 50 to 60% [38, 41, 42]. While defects in neuronal excitability were reported in one study [42] to date, no major brain anatomical phenotypes have been reported in published studies of heterozygous animals [38, 41, 42]. The differences between distinct experimental systems could suggest either species specific differences or disparities between acute knockdown *in vitro* in contrast to dysregulation of ASH1L *in vivo* where compensation mechanisms could be at play.

Next, we determined whether acute knockdown of *ASH1L* could affect neuronal morphogenesis. We assessed changes in neuronal morphogenesis by analyzing neurite

length, branching, changes in morphology at the growing tips of the neurites, and soma size. Cortical neurons were co-transfected with a GFP construct plus either a control Luciferase-shRNA construct or the ASH1L-shRNA construct, and after puromycin selection were immunostained with the pan-neuronal marker β-III-Tubulin to confirm that GFP positive cells were neuronal cells (Fig. 2A). Morphometric analyses done using the GFP channel after confirming expression of β-III-Tubulin showed a 40.5% significant decrease in mean neurite length in male cortical neurons transfected with ASH1L-shRNA compared to controls. Similarly, we find a significant reduction of 59.5% in mean branching complexity index (measure of arborization) in ASH1L knockdown neurons compared to control neurons (Fig. 2B–C). Thus, in human neurons ASH1L depletion decreases neurite outgrowth and branching, suggesting that ASH1L modulates molecular mechanisms governing neuronal morphogenesis. Since we observed similar effects in neurite outgrowth with all ASH1L-shRNA constructs, and the branching complexity index is significantly smaller in ASH1L-shRNA2 neurons, all subsequent experiments were carried out using the ASH1L-shRNA2 construct (ASH1L-shRNA).

We also uncovered the presence of enlarged phalloidin positive structures at the growing tips of the neurites in the ASH1L knockdown neurons. These structures were identified using phalloidin staining in combination with β-III-Tubulin staining in human neurons (Fig. 2D). Analysis of the area and integrated density showed a significant increase in phalloidin staining areas under ASH1L knockdown conditions compared to controls (Fig. 2E and Supplementary Figure S2E). This suggests, knockdown of ASH1L could interfere with normal morphology leading to a re-arrangement of actin filaments [43]. Alternatively, reduction in neurite growth has been correlated with growth cone enlargement in *Aplysia* neurons [44], so the enlargement of phalloidin-positive structures at the growing tips of neurites with ASH1L knockdown could reflect the reduced neurite length observed in human neurons.

Similarly, changes in neuronal morphology have been correlated with alterations in soma size [45, 46]. We analyzed the size of the cell soma in neurons with knockdown for ASH1L compared to control neurons. We find a modest but significant 1.3-fold increase in cell soma area (Fig. 2F) in neurons with ASH1L knockdown compared to control neurons. Thus, we identified an additional morphological effect (increased soma size) of dysregulating ASH1L that correlates with changes in neuronal morphology.

To ensure that the morphological changes observed were not a consequence of changes in cell fate we compared the neuronal composition of control and ASH1L knockdown cultures. We used β-III-Tubulin as a pan-neuronal marker, DCX as a marker of immature neurons, and CTIP2 as a marker for deeper layer cortical excitatory neurons (Supplementary Figure S2F). We analyzed neurons between days 32 to 33 of neuronal induction and found no significant difference in the percentage of either β-III-Tubulin, CTIP2 or DCX positive cells in control *vs.* ASH1L knockdown cultures (Supplementary Figure S2F). Similarly, analysis of the proportion of GFP positive cells that were simultaneously positive for either CTIP2 or β-III-Tubulin positive showed no significant difference between ASH1L knockdown *vs.* control neurons (Fig. 2G–H and Supplementary Figure S2G–H). However, we found an increase of over 9% in the percentage of GFP+/DCX+ neurons with ASH1L knockdown

compared to controls (Supplementary Figure S2G–H). Together these data suggest that while knockdown of ASH1L does not appear to change the cell fate of the neurons it could delay their maturation. Our experimental system is representative of early stages in neuronal development. The reduction in neurite outgrowth correlates with an increased ratio of immature neurons. However, whether the delay in maturation could be overcome at later stages of development is an important question that remains to be answered.

PRC2 and ASH1L counteracting activities modulate neuronal morphogenesis

ASH1L is a member of the Trithorax group of chromatin regulatory proteins, which are proposed to modulate gene expression by counteracting Polycomb complex function during development [11, 12]. PRC2 is a major chromatin regulator Polycomb complex that modifies chromatin by tri-methylation of histone H3 on Lysine 27 (H3K27me3), which is a chromatin repressive mark [47]. We hypothesized that PRC2 and ASH1L opposing activities could regulate gene networks that modulate neuronal morphogenesis in human neurons. Thus, we asked whether impairing the catalytic activity of PRC2 in human neurons would counteract the effect of ASH1L knockdown (Supplementary Fig. S3A). We exposed ASH1L-shRNA transfected human neurons to the EZH2 catalytic inhibitor - EI1 [30]. Previous studies in non-neuronal cells have shown differential inhibitory effects of EI1 in EZH2 catalytic activity depending on the dose and length of treatment [30]. Therefore, we treated control and ASH1L-shRNA transfected human neurons with 1.25 and 2.5 μM of EI1 for 3 or 5 days in culture (Fig. 3A–C and Supplementary Fig. S3A to C) [30]. After 3 days of EI1 treatment, there was a significant but modest rescue in neurite length with both doses of EI1 (Fig. 3B), which correlated with a significant difference from the untreated ASH1L-knockdown neurons but did not reach levels similar to the untreated control neurons. After 5 days there was a significant increase in neurite length for both 1.25 and 2.5 μM EI1 treatments, to levels significantly different from the untreated ASH1L-knockdown neurons (Fig. 3C).

Analysis of neurite branching showed that ASH1L knockdown neurons treated with 1.25 μM and 2.5μM EI1 for 5 days had a modest but significant rescue in the number of branches per cell compared to untreated ASH1L-shRNA neurons (Supplementary Fig. S3C). However, no significant effect was observed with either dose after 3 days of treatment (Supplementary Fig. S3B). Therefore, inhibition of the catalytic activity of PRC2 primarily rescues the neurite length phenotype in ASH1L-knockdown neurons and more modestly the branching phenotype. Taken together these findings suggest that there is antagonism between the Trithorax protein ASH1L and the PRC2 complex proteins during the development of neuronal arbors, being determined by this balance.

ASH1L specifically regulates the expression of the neurotrophin receptor TrkB and its isoforms

The antagonizing activities of ASH1L and PRC2 could regulate gene programs important for neuronal morphogenesis. As neurotrophin-signaling is essential for neuronal arborization [48], we used the ENCODE database to determine if epigenetic marks associated with transcriptional activation or repression are present in the neurotrophin receptors, *NTRK1* (TrkA), *NTRK2* (TrkB), *NTRK3* (TrkC) and *P75* (P75) [49]. Using data available for human stem cell derived cortical excitatory neurons, we aligned each gene to epigenetic marks

associated with transcriptional repression by PRC2 (H3K27me3) [50], and associated with active gene transcription (H3K36me3 and H3K4me3) [51–53]. The current ENCODE data sets lack analysis of H3K36me2 which is primarily deposited by ASH1L. However, H3K36me2 presence will lead to upregulation of H3K36me3 by SET2 [54], and H3K4me3 marks are deposited by the ASH1L interactor - MLL complex [55]. Therefore, both H3K36me3 and H3K4me3 marks served as correlative evidence for the presence of H3K36me2 marks [56]. We found that both NTRK1 and NTRK3 are enriched for the PRC2 associated H3K27me3 epigenetic marks along the gene body, while P75 shows high enrichment in H3K27me3 marks at its transcription start site. In contrast, NTRK2 is primarily enriched in H3K36me3 along the gene body and H3K4me3 closer to the promoter regions (Supplementary Fig. S3D). These results suggest that in human neurons NTRK1, NTRK3 and P75 expression could be suppressed by PRC2. However, the absence of H3K27me3 marks on NTRK2, suggest that under normal conditions NTRK2 is not repressed by PRC2 and hence NTRK2 is actively transcribed in neurons under normal conditions. To determine if ASH1L could differentially modulate the expression of all neurotrophin receptors, we evaluated their mRNA levels using RT-qPCR analyses on cortical neurons that were transfected with control and ASH1L-shRNA constructs. Knockdown of ASH1L in cortical neurons is associated with a 41.8% significant decrease in NTRK2 mRNA, but did not alter NTRK1, NTRK3 or P75 mRNA levels (Fig. 3D). Since, binding of BDNF to its TrkB receptor is essential for neuronal arborization [57], this raises the possibility that the epigenetic regulation of TrkB by ASH1L could modulate neuronal morphogenesis.

The finding that ASH1L regulates the expression of TrkB posits the question of whether there is a direct correlation between the rescue of neuronal arborization by EZH2 inhibition and the regulation of TrkB gene expression by ASH1L. Therefore, we analyzed changes in the levels of TrkB gene expression in response to EZH2 inhibition in neurons with ASH1L knockdown (Supplementary Fig. S3E). Neurons were analyzed for gene expression after a 5-day treatment because we observed a larger rescue effect under this treatment (Fig. 3C). Comparison of untreated *vs.* 2.5μM EI1 treated ASH1L-knockdown neurons showed an upward but variable trend in expression of NTRK2. Thus, suggesting that the rescue by EZH2 inhibition of ASH1L phenotypes might implicate additional pathways aside from the BDNF-TrkB signaling pathway. As TrkB has several functional variants generated by alternative splicing, we next evaluated the effect of ASH1L knockdown on NTRK2 splice variant expression.

Histone H3K36 methylation regulates pre-mRNA splicing in *S. cerevisiae* [58], and MRG15, which forms a complex with ASH1L [59], also regulates pre-mRNA splicing [60]. Since ASH1L dimethylates H3K36 [12, 55] and forms a complex with MRG15, we asked if ASH1L could regulate the alternative splicing of NTRK2 (TrkB) mRNA, which has seven distinct splicing isoforms [61, 62]. Four of these isoforms are expressed in the human PFC during postnatal development [62]. Because our cultures are composed of forebrain cortical neurons [17, 19], we focused on 3 isoforms expressed in the PFC for which their sequence was amenable to PCR based detection (Fig. 3E–F and Supplementary Table S11). Using ddPCR in control and ASH1L shRNA-transfected neurons, we found a significant decrease in expression of isoforms containing exons 5 and 6 (NTRK2 e5/6), which includes the full length TrkB (NTRK2-FL) and all isoforms that contain the N-terminus of the TrkB

protein. Two additional isoforms that we examined were TrkB-T1 (NTRK2 e15/16) [61] and TrkB-SHC (NTRK2 e17/19) [63]. TrkB-T1 lacks the tyrosine kinase domain, SHC, and PLCγ binding domains. TrkB-T1 acts as a dominant negative that scavenges the full length TrkB, leading to decreased BDNF-TrkB signaling [62] and has been suggested to contribute to neuronal arborization [64]. TrkB-SHC contains the SHC binding domain, but lacks the PLCγ binding domain and the tyrosine kinase domain, and has been proposed to decrease the levels of phosphorylated TrkB [62, 63] which in turn could lead to reduced neuronal arborization [29]. We found a significant downregulation of isoform NTRK2 e15/16, which encodes TrkB-T1. However, we found significant upregulation of NTRK2 e17/19, which encodes TrkB-SHC. Mice with a loss of function TrkB-T1 have reduced dendritic complexity [64]. Taken together these data suggest that ASH1L modulates the expression of full length TrkB and differentially regulates two other N-terminus containing isoforms, TrkB-T1 and TrkB-SHC, which could further exacerbate the neuronal morphogenesis phenotype based on their opposing effects in neuronal arborization. Downregulation of TrkB-T1 could contribute to the reduced arborization phenotype as this isoform positively regulates neuronal arborization. Upregulation of TrkB-SHC which is a negative regulator of TrkB phosphorylation could further reduce neurite outgrowth and branching.

Exogenous addition of BDNF neurotrophin does not rescue ASH1L neuronal phenotypes and shows impaired downstream activation of CREB signaling

BDNF binding to TrkB receptor will elicit the endocytosis of the receptor bound ligand and in turn elicit a signaling cascade that leads to the phosphorylation and subsequent nuclear translocation of the CREB transcription factor. CREB activation promotes the transcription of both BDNF and TrkB [65, 66]. Additionally, BDNF has been shown to elicit local translation in dendritic and axonal compartments [67]. BDNF treatment was previously used as a rescue strategy in human neurons with defects in BDNF/TrkB signaling to restore neuronal arborization phenotypes [19]. Human stem cell-derived neurons are known to express BDNF in culture; however, the endogenous BDNF may not be sufficient to elicit a TrkB response in ASH1L depleted neurons. Therefore, we sought to augment BDNF/TrkB signaling by supplying exogenous BDNF at receptor saturating levels (10ng/ml) to test if additional BDNF ligand might rescue the neurite growth deficit seen with ASH1L depletion by inducing TrkB expression [68, 69]. We treated control and ASH1L-shRNA transfected neurons for 72 hrs. with 10ng/ml of BDNF (Supplementary Fig. S4A) [19]. In control neurons, we find after long-term exposure to exogenously added BDNF, there is a significant 15% increase in mean neurite length, and a 35% increase in mean branch number, indicating that the TrkB receptors are not saturated with endogenous BDNF (Fig. 4A–C). However, in ASH1L knockdown neurons the addition of exogenous BDNF caused a very modest increase in mean neurite length and branching that was not statistically different from untreated ASH1L knockdown neurons (Fig. 4A–C). Since exogenous BDNF cannot fully rescue neurite phenotype in ASH1L knockdown neurons, this (in addition to EZH2 inhibition) also suggests additional pathways aside from the BDNF-TrkB signaling pathway may be involved.

The inability of exogenous BDNF to fully rescue ASH1L neuronal morphogenesis phenotypes, posits the question of whether the downstream signaling pathway remains

intact after downregulation of ASH1L. BDNF-dependent activation of TrkB is known to induce activation and nuclear translation of the transcription factor CREB through its phosphorylation [70]. Phosphorylated CREB is needed to activate transcription of genes important for neurite outgrowth and neuronal morphogenesis [71, 72]. Thus, we reasoned that if TrkB signaling were intact in the ASH1L depleted neurons, BDNF stimulation would increase nuclear localization of phospho-CREB. shRNA transfected neurons were acutely treated with BDNF at increasing doses (0, 10, 25 and 50 ng/ml) after puromycin selection (Fig. 4D and Supplementary Fig. S4B). We found significant increase in nuclear phospho-CREB signal in control neurons treated with increased BDNF doses. However, in ASH1L knockdown neurons increased BDNF levels did not increase nuclear phospho-CREB signal compared to the untreated control (Fig.4D). Using super resolution microscopy, we find a distinct nuclear localization for phospho-CREB after 25 ng/ml BDNF exposure in control neurons compared to reduced nuclear localization of phospho-CREB in ASH1L knockdown neurons (Fig. 4E). We wondered if the decrease in phospho-CREB signal might be indicative of reduced expression of CREB itself. However, after knockdown of ASH1L in cortical neurons we found no significant change in mRNA levels of *CREB1,* the gene encoding CREB (Supplementary Fig.S4C). Taken together, these findings show that CREB gene expression is maintained despite the knockdown of ASH1L, but the reduction of ASH1L results in decreased activation of CREB by BDNF.

CREB phosphorylation can be regulated independent of the BDNF/TrkB signaling pathway. Therefore, we sought to define whether other genes relevant to the CREB-signaling pathway were altered. We examined the expression of c-FOS, MSK1, GSK3β and CAMKIV in control and ASH1L knockdown neurons in the absence of exogenous BDNF. MSK1, GSK3β and CAMKIV phosphorylate CREB leading to its activation [73], while c-FOS is transcribed in response to CREB phosphorylation [74]. We found no significant change in MSK1, GSK3β or c-FOS gene expression, but we observed increased levels of CAMKIV in ASH1L knockdown neurons (Supplementary Figure S4D). However, the increase in CAMKIV gene expression was not sufficient to increase CREB activity as we observed no change in c-FOS gene expression.

DISCUSSION

In mice, ASH1L is essential for embryonic development, as ASH1L$^{-/-}$ mice are early embryonic lethal [38]. While ASH1L$^{-/+}$ mice had no major brain abnormalities reported [38], they did show changes in gene expression in response to neuronal activity [38]. RNA interference of the *ASH1L* homologue (*Ash1*) in *Drosophila* disrupted their capacity to complete habituation tasks, suggesting a disruption of neuronal function [9]. The *Drosophila* findings are further corroborated by a conditional knockout of ASH1L in mouse that presented autism-like behaviors [40]. However, the extent to which ASH1L contributes to the structural development of human neuronal circuitry is largely unknown. We find that acute knockdown of ASH1L stunts neurite growth and reduces neurite branching in male human stem cell-derived cortical neurons. Our work also suggests that deficits in ASH1L could delay neuronal maturation, as we find that ASH1L knockdown leads to higher percentage of immature neurons. These findings are now corroborated by studies using

CRISPR-knockdown strategies that classify ASH1L in a subset of ASD-risk genes that disrupt neuronal maturation in dopaminergic neurons [75].

The reduced neurite outgrowth is accompanied by enlarged phalloidin areas at the growing ends of the neurons, suggesting that reduction in ASH1L could lead to slower growth rates or could lead to neuronal guidance defects *in vivo* [76]. Alternatively, deficits in ASH1L could be interfering with normal neuronal morphology causing a rearrangement of actin filaments that are observed as enlarged phalloidin regions. In the cultures and transfected cell populations we studied, the majority of cells are neurons. Therefore, we posit that in our system the effect of ASH1L on neuronal morphogenesis is primarily neuronal. However, our findings do not exclude the possibility that dysregulation of ASH1L in other brain cell types could also contribute to the neurological phenotypes in patients with ASH1L mutations.

Several ASD related syndromes associated with defects in BDNF-TrkB signaling, present reduced neurite outgrowth and synaptic defects [29, 77, 78]. *Ash1l* knockout mouse [40, 79], showed ASD-like behaviors and in response to neuronal activity, ASH1L regulates the expression of Neurexin-1α [38]. We posit that similar to other ASD-related syndromes, in humans ASH1L deficits could also lead to defects in synapse development and function. The present work focused on early stages of neuronal development at which human neurons are not synaptically mature. Therefore, assessing the role ASH1L plays in the regulation of synaptic function in long-term cultures of human neurons is an important future direction. Furthermore, defining the role of ASH1L in mature neurons will also inform on whether the defects in neuritogenesis, and soma size observed in immature neurons associated with loss of ASH1L are transitory phenotypes.

The present work has focused on studying the role of ASH1L in human cortical excitatory neurons. However, based on ASH1L's expression at different stages of neuronal development and in different cell types, mutations in ASH1L could also affect the neuronal progenitor population. A recent multiplex analysis of loss-of-function mutations in several ASD-risk genes identified a class of genes, including ASH1L, that when disrupted in human stem cells led to reduced neuronal numbers [80]. Similarly, CRISPR-knockdown of a subset of ASD-risk genes, including ASH1L, in a mesenchymal neuronal progenitor cell line that gives rise to dopaminergic neurons showed dysregulation of cell cycle genes by transcriptome analysis [75]. These findings suggest a role for ASH1L in neuronal progenitors beyond the phenotypes we find with respect to neuronal morphogenesis and maturation in cortical excitatory neurons.

Our correlation analysis of the top positively co-expressing genes with ASH1L shows an overrepresentation of genes involved in neurite outgrowth and cytoskeletal function. In fact, we further identified that one potential mechanism underlying the neuronal phenotypes associated with ASH1L knockdown is the reduction of the BDNF-TrkB signaling pathway by downregulation of the gene encoding the TrkB receptor and differential regulation of two key isoforms TrkB-T1 and TrkB-SHC. Downregulation of TrkB-T1, a positive regulator of neuronal arborization [64, 81] could provide an additive effect to the reduction in neuronal arborization in ASH1L knockdown neurons. TrkB-SHC negatively modulates TrkB phosphorylation [63] and could impair neuronal arborization. Thus, the upregulation of

TrkB-SHC would ensure that neuronal arborization dependent on the TrkB-BDNF signaling pathway is further repressed in neurons with deficits in ASH1L.

Furthermore, our acute BDNF signaling experiments showed that reduction in TrkB gene expression, leads to a reduced response to BDNF as downregulation of ASH1L leads to diminished levels of nuclear phospho-CREB signal. Since the BDNF-TrkB signaling pathway is critical for neuronal arborization, our findings suggest that ASH1L is important for the early steps of neuronal circuitry development, including neuronal arborization. BDNF regulation of neuronal arborization has been recently suggested to be cell type specific [82]. In our studies, BDNF fails to rescue the neuronal arborization phenotype. However, we find no significant changes in neuronal cell type in the transfected cells. Therefore, the lack of rescue by BDNF is not a result in changes in cell type but could be due to the downregulation of TrkB expression. ASH1L has multiple targets as an epigenetic regulator, but our data indicate that its regulation of the BDNF-TrkB signaling pathway likely contributes to its role in neuronal morphogenesis.

In vivo and *in vitro* evidence suggest that ASH1L contributes to the methylation of H3K4 and H3K36 [32, 83]. The di-methylation of H3K36 (H3K36me2) and trimethylation of H3K4 (H3K4me3) sites modify chromatin structure, allowing for transcriptional activation of target genes [12, 55]. Methylation of H3K36 has been proposed to counteract the activity of the Polycomb group and prevent deposition of the transcriptionally repressive H3K27me3 mark [11]. ASH1L deposition of the H3K36me2 mark has been reported to inhibit the catalytic activity of PRC2 [13]. This mechanism of opposing activities of the Polycomb and Trithorax complex is essential during organogenesis [11]. For example, the PRC2 complex through the tri-methylation of H3K27 regulates cell fate transitions during corticogenesis [15]. In particular, deletion of EZH2, the PRC2 catalytic subunit [11] early in development leads to precocious neuronal differentiation and astrogliogenesis [14]. In addition to its role in cell fate determination, EZH2 has been implicated in neuronal arborization, as knockdown of EZH2 results in increased branching of neuronal arbors in hippocampal neurons and modulated BDNF expression [16]. We find that human PRC2 contributes to development of neuronal arbors, as inhibition of EZH2 rescues primarily the neurite outgrowth phenotypes associated with ASH1L knockdown. We also find an upward but variable trend in the expression of NTRK2 after rescue with EZH2 on ASH1L knockdown neurons. Based on these data, we hypothesize that in the absence of ASH1L, the activating H3K36me2 marks on genes relevant to neuronal morphogenesis and function are reduced, enabling PRC2 to place repressive H3K27me3 marks and reduce the expression of gene programs that regulate neuronal morphogenesis and function (Fig. 4F). Taken together, our findings point to the counteracting activities of ASH1L and PRC2 as modulators of gene networks associated with the development of neuronal connectivity by modulating neuronal morphogenesis

A recent clinical study of a patient with an ASH1L mutation reported that while head circumference was normal at birth it was reduced at 4 years, suggesting a postnatal reduction in brain size or microcephaly [10]. Postnatal microcephaly could arise as a result of impaired neuronal arborization and/or a defect in the generation, proliferation or survival of glial cells or their precursor cells [39, 84]. Deficits in proliferation of glial precursor cells could reflect cell cycle defects, similar to primary/congenital microcephaly, which is associated with

defects in genes involved in cell division that could impair neuronal progenitor proliferation and expansion [85]. Our co-expression analysis in the DFC showed a small cluster of cell cycle genes to be oppositely correlated with ASH1L expression. Similarly, analysis of a mesencephalic derived neural progenitor-like line identified ASH1L as part of a group of ASD-risk genes that had dysregulation of cell cycle pathways [75]. However, to date no analysis of gliogenesis in published ASH1L mutant mouse models has been reported [38, 40–42]. Therefore, whether or not a reduction in glial cells could contribute to the decrease in brain size associated with ASH1L deficits *in vivo* is unknown.

Recently, ASH2L, a member of the Trithorax core complex "COMPASS", was implicated in cell fate transitions during murine cortical development [86]. Since we did not knockdown ASH1L at the neuronal progenitor stage we do not discount the potential of ASH1L to be involved in cell fate transitions during human corticogenesis. Finally, while the current work has focused on the ASH1L- PRC2 axis, it does not escape our attention that ASH1L could also oppose the activity of the PRC1 complex during embryonic development. PRC1 also acts antagonistically to Trithorax protein complexes, and in *Drosophila,* the PRC1 complex regulates neuronal arborization of class IV sensory neurons [87]. Our results combined with these recent studies provide the initial mechanistic insights for understanding the role of epigenetic regulation of neuronal morphogenesis.

Supplementary Material

Refer to Web version on PubMed Central for supplementary material.

ACKNOWLEDGEMENTS

We thank Jeff Twiss for critically reading the manuscript, Amar Kar for insightful discussions on this work, and members of the Twiss laboratory for advice and training on ddPCR. iPSC line 20b was a kind gift of Dr. Kevin Eggan (Harvard Medical School). This work was supported in part by the Center of Biomedical Excellence Dietary Supplements and Inflammation-NIGMS P20GM103641,SC INBRE NIGMS P20GM103499, the SC EPSCoR/IDeA Program under award number 18-SR04 to S.B.L. The views, perspective, and content do not necessarily represent the official views of the SC EPSCoR/IDeA Program. JSL is supported by 1R01NS104428-01A1. Diagram illustrations were made using BioRender.com

REFERENCES

1. Kuehner JN, Bruggeman EC, Wen Z, Yao B. Epigenetic Regulations in Neuropsychiatric Disorders. Front Genet 2019; 10: 268. [PubMed: 31019524]
2. Lamonica JM, Zhou Z. Disentangling chromatin architecture to gain insights into the etiology of brain disorders. Curr Opin Genet Dev 2019; 55: 76–81. [PubMed: 31323465]
3. Abrahams BS, Arking DE, Campbell DB, Mefford HC, Morrow EM, Weiss LA et al. SFARI Gene 2.0: a community-driven knowledgebase for the autism spectrum disorders (ASDs). Mol Autism 2013; 4(1): 36. [PubMed: 24090431]
4. De Rubeis S, He X, Goldberg AP, Poultney CS, Samocha K, Cicek AE et al. Synaptic, transcriptional and chromatin genes disrupted in autism. Nature 2014; 515(7526): 209–215. [PubMed: 25363760]
5. Wang T, Guo H, Xiong B, Stessman HA, Wu H, Coe BP et al. De novo genic mutations among a Chinese autism spectrum disorder cohort. Nat Commun 2016; 7: 13316. [PubMed: 27824329]
6. Tammimies K, Marshall CR, Walker S, Kaur G, Thiruvahindrapuram B, Lionel AC et al. Molecular Diagnostic Yield of Chromosomal Microarray Analysis and Whole-Exome Sequencing in Children With Autism Spectrum Disorder. JAMA 2015; 314(9): 895–903. [PubMed: 26325558]

7. Faundes V, Newman WG, Bernardini L, Canham N, Clayton-Smith J, Dallapiccola B et al. Histone Lysine Methylases and Demethylases in the Landscape of Human Developmental Disorders. Am J Hum Genet 2018; 102(1): 175–187. [PubMed: 29276005]
8. Faundes V, Santa Maria L, Morales P, Curotto B, Alliende MA. [Microarrays in 236 patients with neurodevelopmental disorders and congenital abnormalities]. Rev Med Chil 2017; 145(7): 854–861. [PubMed: 29182193]
9. Stessman HA, Xiong B, Coe BP, Wang T, Hoekzema K, Fenckova M et al. Targeted sequencing identifies 91 neurodevelopmental-disorder risk genes with autism and developmental-disability biases. Nat Genet 2017; 49(4): 515–526. [PubMed: 28191889]
10. Okamoto N, Miya F, Tsunoda T, Kato M, Saitoh S, Yamasaki M et al. Novel MCA/ID syndrome with ASH1L mutation. Am J Med Genet A 2017; 173(6): 1644–1648. [PubMed: 28394464]
11. Schuettengruber B, Bourbon HM, Di Croce L, Cavalli G. Genome Regulation by Polycomb and Trithorax: 70 Years and Counting. Cell 2017; 171(1): 34–57. [PubMed: 28938122]
12. Miyazaki H, Higashimoto K, Yada Y, Endo TA, Sharif J, Komori T et al. Ash1l methylates Lys36 of histone H3 independently of transcriptional elongation to counteract polycomb silencing. PLoS Genet 2013; 9(11): e1003897. [PubMed: 24244179]
13. Huang C, Zhu B. Roles of H3K36-specific histone methyltransferases in transcription: antagonizing silencing and safeguarding transcription fidelity. Biophys Rep 2018; 4(4): 170–177. [PubMed: 30310854]
14. Corley M, Kroll KL. The roles and regulation of Polycomb complexes in neural development. Cell Tissue Res 2015; 359(1): 65–85. [PubMed: 25367430]
15. Pereira JD, Sansom SN, Smith J, Dobenecker MW, Tarakhovsky A, Livesey FJ. Ezh2, the histone methyltransferase of PRC2, regulates the balance between self-renewal and differentiation in the cerebral cortex. Proc Natl Acad Sci U S A 2010; 107(36): 15957–15962. [PubMed: 20798045]
16. Qi C, Liu S, Qin R, Zhang Y, Wang G, Shang Y et al. Coordinated regulation of dendrite arborization by epigenetic factors CDYL and EZH2. J Neurosci 2014; 34(13): 4494–4508. [PubMed: 24671995]
17. Shi Y, Kirwan P, Smith J, Robinson HP, Livesey FJ. Human cerebral cortex development from pluripotent stem cells to functional excitatory synapses. Nat Neurosci 2012; 15(3): 477–486, S471. [PubMed: 22306606]
18. Shi Y, Kirwan P, Livesey FJ. Directed differentiation of human pluripotent stem cells to cerebral cortex neurons and neural networks. Nat Protoc 2012; 7(10): 1836–1846. [PubMed: 22976355]
19. Lizarraga SB, Ma L, Maguire AM, van Dyck LI, Wu Q, Ouyang Q et al. Human neurons from Christianson syndrome iPSCs reveal mutation-specific responses to rescue strategies. Sci Transl Med 2021; 13:580:1–14 [Google Scholar]
20. Laugesen A, Hojfeldt JW, Helin K. Molecular Mechanisms Directing PRC2 Recruitment and H3K27 Methylation. Mol Cell 2019; 74(1): 8–18. [PubMed: 30951652]
21. Gonzalez A, Moya-Alvarado G, Gonzalez-Billaut C, Bronfman FC. Cellular and molecular mechanisms regulating neuronal growth by brain-derived neurotrophic factor. Cytoskeleton (Hoboken) 2016; 73(10): 612–628. [PubMed: 27223597]
22. Yoshii A, Constantine-Paton M. Postsynaptic BDNF-TrkB signaling in synapse maturation, plasticity, and disease. Dev Neurobiol 2010; 70(5): 304–322. [PubMed: 20186705]
23. Miller JA, Ding SL, Sunkin SM, Smith KA, Ng L, Szafer A et al. Transcriptional landscape of the prenatal human brain. Nature 2014; 508(7495): 199–206. [PubMed: 24695229]
24. Hawrylycz MJ, Lein ES, Guillozet-Bongaarts AL, Shen EH, Ng L, Miller JA et al. An anatomically comprehensive atlas of the adult human brain transcriptome. Nature 2012; 489(7416): 391–399. [PubMed: 22996553]
25. Chen J, Bardes EE, Aronow BJ, Jegga AG. ToppGene Suite for gene list enrichment analysis and candidate gene prioritization. Nucleic Acids Res 2009; 37(Web Server issue): W305–311. [PubMed: 19465376]
26. Ludwig TE, Bergendahl V, Levenstein ME, Yu J, Probasco MD, Thomson JA. Feeder-independent culture of human embryonic stem cells. Nat Methods 2006; 3(8): 637–646. [PubMed: 16862139]

27. Thomson JA, Itskovitz-Eldor J, Shapiro SS, Waknitz MA, Swiergiel JJ, Marshall VS et al. Embryonic stem cell lines derived from human blastocysts. Science 1998; 282(5391): 1145–1147. [PubMed: 9804556]
28. Boulting GL, Kiskinis E, Croft GF, Amoroso MW, Oakley DH, Wainger BJ et al. A functionally characterized test set of human induced pluripotent stem cells. Nat Biotechnol 2011; 29(3): 279–286. [PubMed: 21293464]
29. Ouyang Q, Lizarraga SB, Schmidt M, Yang U, Gong J, Ellisor D et al. Christianson syndrome protein NHE6 modulates TrkB endosomal signaling required for neuronal circuit development. Neuron 2013; 80(1): 97–112. [PubMed: 24035762]
30. Qi W, Chan H, Teng L, Li L, Chuai S, Zhang R et al. Selective inhibition of Ezh2 by a small molecule inhibitor blocks tumor cells proliferation. Proc Natl Acad Sci U S A 2012; 109(52): 21360–21365. [PubMed: 23236167]
31. Pillai AG, de Jong D, Kanatsou S, Krugers H, Knapman A, Heinzmann JM et al. Dendritic morphology of hippocampal and amygdalar neurons in adolescent mice is resilient to genetic differences in stress reactivity. PLoS One 2012; 7(6): e38971. [PubMed: 22701737]
32. Gregory GD, Vakoc CR, Rozovskaia T, Zheng X, Patel S, Nakamura T et al. Mammalian ASH1L is a histone methyltransferase that occupies the transcribed region of active genes. Mol Cell Biol 2007; 27(24): 8466–8479. [PubMed: 17923682]
33. De I, Muller CW. Unleashing the Power of ASH1L Methyltransferase. Structure 2019; 27(5): 727–728. [PubMed: 31067442]
34. Bonfante E, Koenig MK, Adejumo RB, Perinjelil V, Riascos RF. The neuroimaging of Leigh syndrome: case series and review of the literature. Pediatr Radiol 2016; 46(4): 443–451. [PubMed: 26739140]
35. Kim YS, Leventhal BL, Koh YJ, Fombonne E, Laska E, Lim EC et al. Prevalence of autism spectrum disorders in a total population sample. Am J Psychiatry 2011; 168(9): 904–912. [PubMed: 21558103]
36. Shen W, Krautscheid P, Rutz AM, Bayrak-Toydemir P, Dugan SL. De novo loss-of-function variants of ASH1L are associated with an emergent neurodevelopmental disorder. Eur J Med Genet 2019; 62(1): 55–60. [PubMed: 29753921]
37. Guo H, Wang T, Wu H, Long M, Coe BP, Li H et al. Inherited and multiple de novo mutations in autism/developmental delay risk genes suggest a multifactorial model. Mol Autism 2018; 9: 64. [PubMed: 30564305]
38. Zhu T, Liang C, Li D, Tian M, Liu S, Gao G et al. Histone methyltransferase Ash1L mediates activity-dependent repression of neurexin-1alpha. Sci Rep 2016; 6: 26597. [PubMed: 27229316]
39. Seltzer LE, Paciorkowski AR. Genetic disorders associated with postnatal microcephaly. Am J Med Genet C Semin Med Genet 2014; 166C(2): 140–155. [PubMed: 24839169]
40. Gao Y, Duque-Wilckens N, Aljazi MB, Wu Y, Moeser AJ, Mias GI et al. Loss of histone methyltransferase ASH1L in the developing mouse brain causes autistic-like behaviors. Commun Biol 2021; 4(1): 756. [PubMed: 34145365]
41. Brinkmeier ML, Geister KA, Jones M, Waqas M, Maillard I, Camper SA. The Histone Methyltransferase Gene Absent, Small, or Homeotic Discs-1 Like Is Required for Normal Hox Gene Expression and Fertility in Mice. Biol Reprod 2015; 93(5): 121. [PubMed: 26333994]
42. Zhang C, Xu L, Zheng X, Liu S, Che F. Role of Ash1l in Tourette syndrome and other neurodevelopmental disorders. Dev Neurobiol 2021;81:71–91. [Google Scholar]
43. Menon S, Gupton SL. Building Blocks of Functioning Brain: Cytoskeletal Dynamics in Neuronal Development. Int Rev Cell Mol Biol 2016; 322: 183–245. [PubMed: 26940519]
44. Ren Y, Suter DM. Increase in Growth Cone Size Correlates with Decrease in Neurite Growth Rate. Neural Plast 2016; 2016: 3497901. [PubMed: 27274874]
45. Huang G, Chen S, Chen X, Zheng J, Xu Z, Doostparast Torshizi A et al. Uncovering the Functional Link Between SHANK3 Deletions and Deficiency in Neurodevelopment Using iPSC-Derived Human Neurons. Front Neuroanat 2019; 13: 23. [PubMed: 30918484]
46. Rooney GE, Goodwin AF, Depeille P, Sharir A, Schofield CM, Yeh E et al. Human iPS Cell-Derived Neurons Uncover the Impact of Increased Ras Signaling in Costello Syndrome. J Neurosci 2016; 36(1): 142–152. [PubMed: 26740656]

47. Albert M, Kalebic N, Florio M, Lakshmanaperumal N, Haffner C, Brandl H et al. Epigenome profiling and editing of neocortical progenitor cells during development. EMBO J 2017; 36(17): 2642–2658. [PubMed: 28765163]
48. Deinhardt K, Chao MV. Shaping neurons: Long and short range effects of mature and proBDNF signalling upon neuronal structure. Neuropharmacology 2014; 76 Pt C: 603–609. [PubMed: 23664813]
49. Deinhardt K, Chao MV. Trk receptors. Handb Exp Pharmacol 2014; 220: 103–119. [PubMed: 24668471]
50. van Mierlo G, Veenstra GJC, Vermeulen M, Marks H. The Complexity of PRC2 Subcomplexes. Trends Cell Biol 2019; 29(8): 660–671. [PubMed: 31178244]
51. Eram MS, Kuznetsova E, Li F, Lima-Fernandes E, Kennedy S, Chau I et al. Kinetic characterization of human histone H3 lysine 36 methyltransferases, ASH1L and SETD2. Biochim Biophys Acta 2015; 1850(9): 1842–1848. [PubMed: 26002201]
52. Balbach ST, Orkin SH. An Achilles' Heel for MLL-Rearranged Leukemias: Writers and Readers of H3 Lysine 36 Dimethylation. Cancer Discov 2016; 6(7): 700–702. [PubMed: 27371576]
53. Shao GB, Chen JC, Zhang LP, Huang P, Lu HY, Jin J et al. Dynamic patterns of histone H3 lysine 4 methyltransferases and demethylases during mouse preimplantation development. In Vitro Cell Dev Biol Anim 2014; 50(7): 603–613. [PubMed: 24619213]
54. Li J, Ahn JH, Wang GG. Understanding histone H3 lysine 36 methylation and its deregulation in disease. Cell Mol Life Sci 2019; 76(15): 2899–2916. [PubMed: 31147750]
55. Zhu L, Li Q, Wong SH, Huang M, Klein BJ, Shen J et al. ASH1L Links Histone H3 Lysine 36 Dimethylation to MLL Leukemia. Cancer Discov 2016; 6(7): 770–783. [PubMed: 27154821]
56. Miao F, Natarajan R. Mapping global histone methylation patterns in the coding regions of human genes. Mol Cell Biol 2005; 25(11): 4650–4661. [PubMed: 15899867]
57. Segal RA, Pomeroy SL, Stiles CD. Axonal growth and fasciculation linked to differential expression of BDNF and NT3 receptors in developing cerebellar granule cells. J Neurosci 1995; 15(7 Pt 1): 4970–4981. [PubMed: 7623126]
58. Sorenson MR, Jha DK, Ucles SA, Flood DM, Strahl BD, Stevens SW et al. Histone H3K36 methylation regulates pre-mRNA splicing in Saccharomyces cerevisiae. RNA Biol 2016; 13(4): 412–426. [PubMed: 26821844]
59. Lee Y, Yoon E, Cho S, Schmahling S, Muller J, Song JJ. Structural Basis of MRG15-Mediated Activation of the ASH1L Histone Methyltransferase by Releasing an Autoinhibitory Loop. Structure 2019; 27(5): 846–852 e843. [PubMed: 30827841]
60. Iwamori N, Tominaga K, Sato T, Riehle K, Iwamori T, Ohkawa Y et al. MRG15 is required for pre-mRNA splicing and spermatogenesis. Proc Natl Acad Sci U S A 2016; 113(37): E5408–5415. [PubMed: 27573846]
61. Fryer RH, Kaplan DR, Feinstein SC, Radeke MJ, Grayson DR, Kromer LF. Developmental and mature expression of full-length and truncated TrkB receptors in the rat forebrain. J Comp Neurol 1996; 374(1): 21–40. [PubMed: 8891944]
62. Luberg K, Wong J, Weickert CS, Timmusk T. Human TrkB gene: novel alternative transcripts, protein isoforms and expression pattern in the prefrontal cerebral cortex during postnatal development. J Neurochem 2010; 113(4): 952–964. [PubMed: 20193039]
63. Wong J, Garner B. Evidence that truncated TrkB isoform, TrkB-Shc can regulate phosphorylated TrkB protein levels. Biochem Biophys Res Commun 2012; 420(2): 331–335. [PubMed: 22425982]
64. Carim-Todd L, Bath KG, Fulgenzi G, Yanpallewar S, Jing D, Barrick CA et al. Endogenous truncated TrkB.T1 receptor regulates neuronal complexity and TrkB kinase receptor function in vivo. J Neurosci 2009; 29(3): 678–685. [PubMed: 19158294]
65. Deogracias R, Espliguero G, Iglesias T, Rodriguez-Pena A. Expression of the neurotrophin receptor trkB is regulated by the cAMP/CREB pathway in neurons. Mol Cell Neurosci 2004; 26(3): 470–480. [PubMed: 15234351]
66. Finkbeiner S Calcium regulation of the brain-derived neurotrophic factor gene. Cell Mol Life Sci 2000; 57(3): 394–401. [PubMed: 10823240]
67. Leal G, Comprido D, Duarte CB. BDNF-induced local protein synthesis and synaptic plasticity. Neuropharmacology 2014; 76 Pt C: 639–656. [PubMed: 23602987]

68. Elliott RC, Black IB, Dreyfus CF. Differential regulation of p75 and trkB mRNA expression after depolarizing stimuli or BDNF treatment in basal forebrain neuron cultures. J Neurosci Res 2001; 66(1): 83–88. [PubMed: 11599004]
69. Esvald EE, Tuvikene J, Sirp A, Patil S, Bramham CR, Timmusk T. CREB Family Transcription Factors Are Major Mediators of BDNF Transcriptional Autoregulation in Cortical Neurons. J Neurosci 2020; 40(7): 1405–1426. [PubMed: 31915257]
70. Watson FL, Heerssen HM, Moheban DB, Lin MZ, Sauvageot CM, Bhattacharyya A et al. Rapid nuclear responses to target-derived neurotrophins require retrograde transport of ligand-receptor complex. J Neurosci 1999; 19(18): 7889–7900. [PubMed: 10479691]
71. Pollscheit J, Glaubitz N, Haller H, Horstkorte R, Bork K. Phosphorylation of serine 774 of the neural cell adhesion molecule is necessary for cyclic adenosine monophosphate response element binding protein activation and neurite outgrowth. J Neurosci Res 2012; 90(8): 1577–1582. [PubMed: 22419107]
72. Spencer TK, Mellado W, Filbin MT. BDNF activates CaMKIV and PKA in parallel to block MAG-mediated inhibition of neurite outgrowth. Mol Cell Neurosci 2008; 38(1): 110–116. [PubMed: 18381242]
73. Wang H, Xu J, Lazarovici P, Quirion R, Zheng W. cAMP Response Element-Binding Protein (CREB): A Possible Signaling Molecule Link in the Pathophysiology of Schizophrenia. Front Mol Neurosci 2018; 11: 255. [PubMed: 30214393]
74. Ahn S, Olive M, Aggarwal S, Krylov D, Ginty DD, Vinson C. A dominant-negative inhibitor of CREB reveals that it is a general mediator of stimulus-dependent transcription of c-fos. Mol Cell Biol 1998; 18(2): 967–977. [PubMed: 9447994]
75. Lalli MA, Avey D, Dougherty JD, Milbrandt J, Mitra RD. High-throughput single-cell functional elucidation of neurodevelopmental disease-associated genes reveals convergent mechanisms altering neuronal differentiation. Genome Res 2020; 30(9): 1317–1331. [PubMed: 32887689]
76. Bakos J, Bacova Z, Grant SG, Castejon AM, Ostatnikova D. Are Molecules Involved in Neuritogenesis and Axon Guidance Related to Autism Pathogenesis? Neuromolecular Med 2015; 17(3): 297–304. [PubMed: 25989848]
77. Sampathkumar C, Wu YJ, Vadhvani M, Trimbuch T, Eickholt B, Rosenmund C. Loss of MeCP2 disrupts cell autonomous and autocrine BDNF signaling in mouse glutamatergic neurons. Elife 2016; 5.
78. Cao C, Rioult-Pedotti MS, Migani P, Yu CJ, Tiwari R, Parang K et al. Impairment of TrkB-PSD-95 signaling in Angelman syndrome. PLoS Biol 2013; 11(2): e1001478. [PubMed: 23424281]
79. Qin L, Williams JB, Tan T, Liu T, Cao Q, Ma K et al. Deficiency of autism risk factor ASH1L in prefrontal cortex induces epigenetic aberrations and seizures. Nat Commun 2021; 12(1): 6589. [PubMed: 34782621]
80. Cederquist GY, Tchieu J, Callahan SJ, Ramnarine K, Ryan S, Zhang C et al. A Multiplex Human Pluripotent Stem Cell Platform Defines Molecular and Functional Subclasses of Autism-Related Genes. Cell Stem Cell 2020; 27(1): 35–49 e36. [PubMed: 32619517]
81. Holt LM, Hernandez RD, Pacheco NL, Torres Ceja B, Hossain M, Olsen ML. Astrocyte morphogenesis is dependent on BDNF signaling via astrocytic TrkB.T1. Elife 2019; 8: 1–27. [Google Scholar]
82. Zagrebelsky M, Godecke N, Remus A, Korte M. Cell type-specific effects of BDNF in modulating dendritic architecture of hippocampal neurons. Brain Struct Funct 2018; 223(8): 3689–3709. [PubMed: 30022251]
83. Xia M, Liu J, Wu X, Liu S, Li G, Han C et al. Histone methyltransferase Ash1l suppresses interleukin-6 production and inflammatory autoimmune diseases by inducing the ubiquitin-editing enzyme A20. Immunity 2013; 39(3): 470–481. [PubMed: 24012418]
84. Cloetta D, Thomanetz V, Baranek C, Lustenberger RM, Lin S, Oliveri F et al. Inactivation of mTORC1 in the developing brain causes microcephaly and affects gliogenesis. J Neurosci 2013; 33(18): 7799–7810. [PubMed: 23637172]
85. Manzini MC, Walsh CA. What disorders of cortical development tell us about the cortex: one plus one does not always make two. Curr Opin Genet Dev 2011; 21(3): 333–339. [PubMed: 21288712]

86. Li L, Ruan X, Wen C, Chen P, Liu W, Zhu L et al. The COMPASS Family Protein ASH2L Mediates Corticogenesis via Transcriptional Regulation of Wnt Signaling. Cell Rep 2019; 28(3): 698–711 e695. [PubMed: 31315048]

87. Parrish JZ, Emoto K, Jan LY, Jan YN. Polycomb genes interact with the tumor suppressor genes hippo and warts in the maintenance of Drosophila sensory neuron dendrites. Genes Dev 2007; 21(8): 956–972. [PubMed: 17437999]

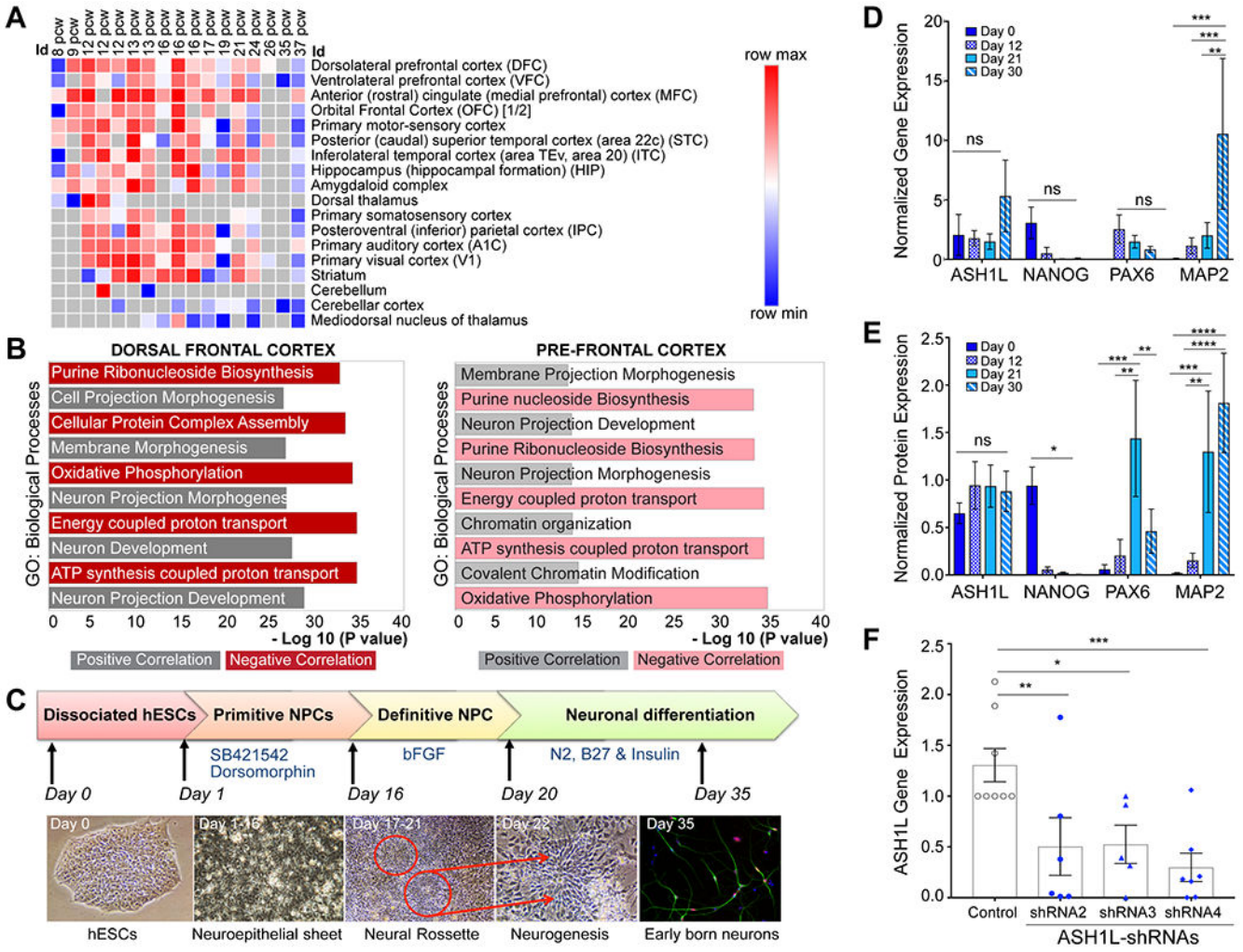

Figure 1. ASH1L is expressed throughout development *in vivo* and *in vitro*.

(**A**) Analysis of ASH1L expression using the Allen Brain Atlas data set across 12 developmental stages and 18 brain structures during prenatal development. Heat map representation of ASH1L expression built using RNA-sequencing expression values downloaded from the developmental transcriptome database for ASH1L. Morpheus Software was used to build the Heat map showing each donor age with the corresponding brain region analyzed. Highest expression values are shown in red and lowest expression values are shown in blue. Grey values are used when no data was available for a particular developmental stage. (**B**) Pathway analysis of top positive correlated and top negative correlated genes with ASH1L during pre-natal development in DFC and PFC. Positive correlative genes with R values above 0.7 or negative correlative genes with R values below −0.7 were identified between 8 to 18 pcw for the DFC and 8 to 37 pcw for the PFC. GO categories for biological processes are shown as the negative Log10 of the adjusted p-value by Bonferroni correction. (**C**) Neuronal differentiation of hESCs into cortical deeper layer neurons. Top panel shows the major cellular stages from day 0 onwards during neuronal differentiation using a double SMAD inhibition protocol. Bottom panel shows corresponding images for each stage including hESCs colony before single cell dissociation

(day 0), a neuroepithelial like sheet (days 1 to 16), the neural rosette stage (days 17-22), and deeper layer neurons (day 35). Deeper layer neurons were identified by co-immunostaining with CTIP2, a layer V marker (red) and β-III-Tubulin a pan-neuronal marker (green). (**D**) Analysis for ASH1L expression is shown at four distinct stages of in vitro neuronal differentiation for male H1 cells (days 0, 12, 21 and 30) in four independent experiments. Normalized gene expression is shown for *ASH1L*, *NANOG*, a stem cell marker, *PAX6*, a neuronal progenitor marker and *MAP2*, a mature neuron marker. Differential gene expression for MAP2 between day 0 to day 30 (***P = 0.0001), day 12 to day 30 (***P = 0.0001) and day 21 to day 30 (**P = 0.0013) by two-way ANOVA. (**E**) MAP2 protein was significantly differentially expressed between Day 0 and Day 21 (***P = 0.0007), Day 0 and Day 30 (****P < 0.0001), Day 12 to Day 21 (**P = 0.0022), and Day 12 to Day 30 (****P < 0.0001). Statistical analysis was carried using two-way ANOVA for multiple comparisons without corrections. (**F**) Gene expression analysis of *ASH1L* by qPCR in control or knockdown conditions. Expression of *ASH1L* normalized to *GAPDH* expression is shown for each experiment. Each data point represents the average of three technical replicates per experiment. Control GFP (open gray circles) = 1.31 ± 0.163, $n = 8$; shRNA-2 (solid blue circles) = 0.504 ± 0.284, $n = 6$; shRNA-3 (solid blue triangles) = 0.525 ± 0.189, $n = 5$; shRNA-4 (solid blue diamonds) = 0.2989 ± 0.1402, n = 7. Ordinary one-way ANOVA uncorrected for multiple comparisons was used to obtain the p-values for: GFP *vs.* shRNA-2 (**P = 0.0069), GFP *vs.* shRNA3 (***P = 0.012) and GFP *vs.* shRNA4 (***P = 0.0008). In all graphs, results are shown as the mean ± standard error of the mean (SEM).

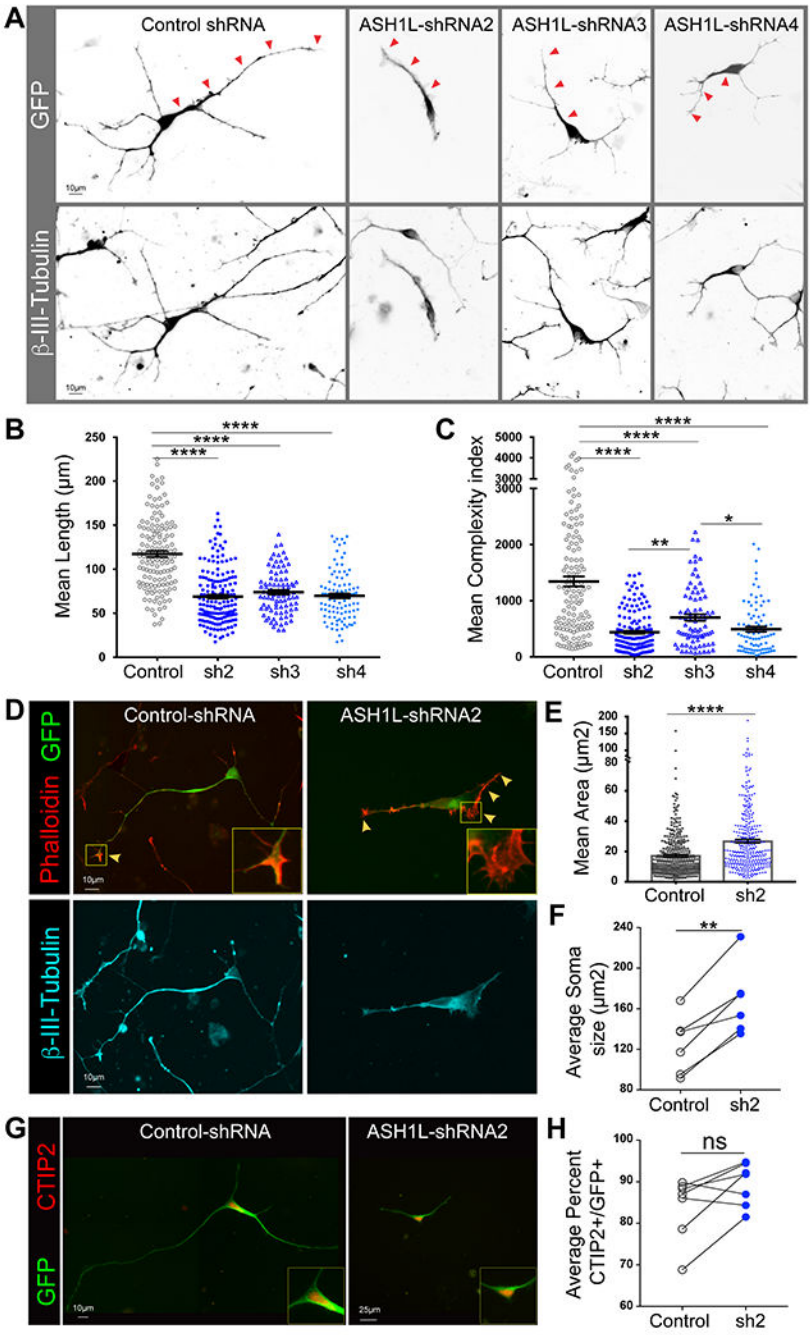

Figure 2. ASH1L modulates neuronal morphogenesis and soma size in cortical excitatory deeper layer neurons but does not alter cell fate *in vitro*.

(**A**) Defects in neurite length are observed upon knockdown of ASH1L in cortical excitatory neurons. Representative images are shown for neurons electroporated at days 28 to 30 with GFP and control or ASH1L-targeting shRNA constructs. Top panels show GFP positive cells and bottom panels show β–III-Tubulin positive cells. For ease of viewing, grey scale images are shown as inverted images. Red arrows follow the longest neurite in the GFP positive neurons. Red boxes highlight regions of branching in the different neurons with an enlarged panel shown on the right of the image. Scale bar, 10μm. Neurons were treated

with puromycin one day after nucleofection and were analyzed 72 hrs. after the start of the puromycin selection at days 32 to 34 of neuronal induction. Neurites stained with β–III-Tubulin were measured using Neurolucida tracing software and no distinction was made between dendrites and axons. (**B**) Mean neurite length in cortical neurons under control or ASH1L knockdown conditions. Control shRNA (open grey circles) = 117.3 ± 3.92, n = 136 cells, N= 3 experiments; shRNA-2 (blue solid circles) = 68.91 ± 2.35, n = 171 cells, N= 6 experiments; shRNA-3 (open blue triangles) = 73.95 ± 2.658, n = 87 cells, N = 3 experiments; shRNA-4 (solid light blue diamonds) = 69.76 ± 2.76, n = 102 cells, N = 3 experiments. Statistical analysis was conducted using ordinary one-way ANOVA uncorrected for multiple comparisons using the uncorrected Fishers LSD's. (****$p < 0.0001$). (**C**) Neurite branching complexity index in control and ASH1L knockdown. Control shRNA (open grey circles) = 1343 ± 89.46, n = 132 cells, N= 3 experiments; shRNA-2 (blue solid circles) = 438.5 ± 29.32, n = 150 cells, N= 6 experiments; shRNA-3 (open blue triangles) = 700.7 ± 58.45, n = 82 cells, N = 3 experiments; shRNA-4 (solid light blue diamonds) = 493.6 ± 47.07, n = 88 cells, N = 3 experiments. shRNA2 *vs.* shRNA 3 ** P < 0.005; shRNA3 *vs.* shRNA4 * P < 0.05. Statistical analysis was conducted using uncorrected Fisher's LSD multiple comparisons with ordinary one-way ANOVA (****P < 0.0001). All measurements were first analyzed for outliers using the ROUT (Q = 1%) method in all conditions and the analysis shown here was conducted after removal of outliers if present. In all graphs, error bars represent SEM, middle lane represents the mean value, and all cell measurements are shown per condition for all experiments. (**D**) Enlarged phalloidin positive areas are observed in neurons knockdown for ASH1L. Representative images are shown for neurons electroporated with GFP and control or ASH1L-targeting shRNA2 (sh2). Top panels show GFP positive cells (green) co-stained with phalloidin (red) and bottom panels show β–III-Tubulin positive cells (cyan). Scale bar, 10μm. Growth cone areas were measured using ImageJ. **(E)** Mean phalloidin positive Area (in μm^2) at ends of growing neurites in control and ASH1L knockdown (N=5 experiments). Control shRNA (open grey circles) = 17.18 ± 0.80, n=468 phalloidin positive areas; shRNA-2 (blue solid circles) = 26.8 ± 1.21, n=337 phalloidin positive areas. Statistical analysis was conducted using unpaired T-test with Welch's correction (****P < 0.0001). (**F**) Mean Soma area size (in μm^2) in control and ASH1L knockdown (N=6 experiments). Each individual data point represents the average value per experiment. Control and knockdown values are shown for each paired experiment. Control shRNA (open black circles) n= 224 cell somas analyzed; shRNA2 (blue solid circles) n= 258 cell somas analyzed. Between 35 to 50 neurons were analyzed per experiment. Statistical analysis was conducted using paired t-test (**P < 0.0015). (**G**) Neurons with ASH1L knockdown remain as deeper layer neurons. Representative images are shown for neurons electroporated at day 28 to day 30 with GFP and control or ASH1L-targeting shRNA constructs. Neurons were treated with puromycin one day after nucleofection and were analyzed 72 hrs. after the start of the puromycin selection (day 32 to 34). Panels show GFP positive cells stained with CTIP2 a marker for layer V deeper layer cortical excitatory neurons (red). For ease of viewing of CTIP2 positive nuclei an enlarged section is shown on the right bottom corner of each image. Scale bars, 10μm and 25μm. (**H**) Mean number of GFP positive neurons that are also positive for CTIP2 in control and ASH1L knockdown (N=7 experiments). Each data point represents the average values per experiment. Control and knockdown are shown as matched paired

experiments. Control shRNA (open black circles), n= 851 GFP+ cells analyzed; shRNA2 (solid blue circles) n=724 GFP+ cells analyzed. Statistical analysis was conducted using a paired t-test (ns=not significant).

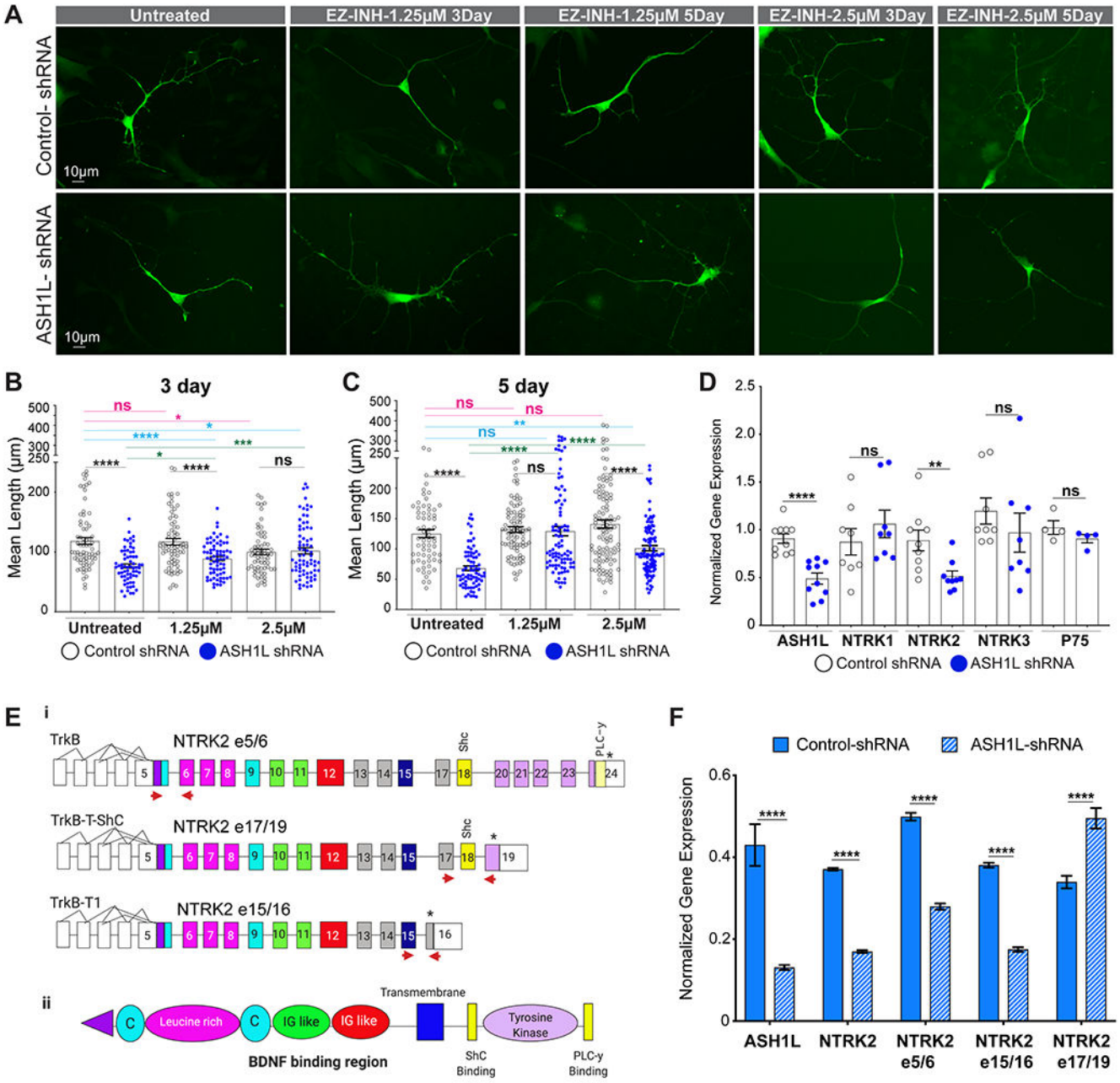

Figure 3. ASH1L phenotype is rescued by EZH2 inhibition and correlates with downregulation of NTRK2.

(**A**) Representative images are shown for neurons electroporated with GFP and either control-shRNA or ASH1L-shRNA constructs treated with 1.25μM or 2.5μM EZH2 inhibitor (EI1) for 3 and 5 days. Scale bars, 10μm. In general, neurons were electroporated at day 29 of neuronal induction. 24 hrs. after electroporation neurons were treated with puromycin. 48 hrs. after the puromycin treatment neurons were treated with an EZH2 inhibitor for 72 hrs. (3-day treatment) or for 120 hrs. (5-day treatment). Neurons were fixed at day 35 of neuronal induction (3-day treatment) or at day 37 of neuronal induction (5-day treatment). See supplementary figure S3B for detail treatment scheme. (**B**) Mean neurite length in

cortical neurons under control or ASH1L knockdown conditions were either untreated or treated for 3 days with 1.25μM or 2.5μM EI1. All measurements per cell are shown for each condition in combination with the mean ± SEM. All control shRNA are open black circles and ASH1L-shRNA are solid blue circles. Control shRNA = 118.3 ± 5.82, n = 70 cells *vs.* ASH1L-shRNA = 76.51 ± 3.45, n = 66 cells; Control-shRNA+1.25μM EI1 = 117.1 ± 5.43, n = 69 cells *vs.* ASH1L-shRNA +1.25μM EI1 = 88.9 ± 3.41, n = 70 cells; Control-shRNA + 2.5μM EI1 = 100.1 ± 4.65, n = 64 cells *vs.* ASH1L-shRNA + 2.5μM EI1 = 101.9 ± 5.30, n = 73 cells. N=3 experiments per condition. Statistical analysis was conducted using ordinary one-way ANOVA for multiple comparisons with Welch's correction. Comparisons between untreated control and EZH2 inhibitor treated controls are in magenta. Comparisons between untreated control and EZH2 inhibitor treated knockdown samples are in cyan. Comparisons between untreated knockdown samples and EZH2 inhibitor treated knockdown samples are in green. ****P < 0.0001; ***P = 0.0001, *P < 0.04, and not significant (ns). (**C**) Mean neurite length in cortical neurons under control or ASH1L knockdown conditions were either untreated or treated for 5 days with 1.25μM or 2.5μM EI1. All control shRNA are open black circles and ASH1L-shRNA are solid blue circles. All measurements per cell are shown for each condition in combination with the mean ± SEM. N= 4 experiments for Untreated and EI1 1.25μM treated groups and 6 experiments for EI1 2.5μM treated groups. Control-shRNA=125.2 ± 6.49, n = 63 cells; ASH1L-shRNA = 68.16 ± 3.807, n = 75 cells; Control-shRNA+1.25μM EI1 = 132.0 ± 4.71, n = 85 cells; ASH1L-shRNA+1.25μM EI1 = 129.3 ± 7.56, n = 94 cells; Control-shRNA + 2.5μM EI1 = 141.0 ± 7.56, n = 107 cells; ASH1L-shRNA + 2.5μM EI1 = 101.1 ± 4.39, n = 102 cells. Statistical analysis was conducted using ordinary one-way ANOVA for multiple comparisons with Welch's correction. Comparisons between untreated control and EZH2 inhibitor treated controls are in magenta. Comparisons between untreated control and EZH2 inhibitor treated knockdown samples are in cyan. Comparisons between untreated knockdown samples and EZH2 inhibitor treated knockdown samples are in green. ****P < 0.0001, **P < 0.003, and not significant (ns). For (B) and (C) data was first analyzed with the ROUT method to account for any outliers (Q=1%). (**D**) Analysis of gene expression across genes encoding the different neurotrophin receptors in control and ASH1L knockdown cortical neurons. qPCR analysis of expression shown as normalized data to reference gene GAPDH that was then normalized to control is shown as normalized ΔΔCt values for control (black open circles) and ASH1L shRNA (blue solid circles) samples for the following genes: ASH1L (n=16 independent experiments, ****P <0.0001); NTRK1 (n = 11 independent experiments, ns); NTRK2 (n=14 independent experiments, **P < 0.0013); NTRK3 (n = 11 independent experiments, ns); and P75 (n=5 independent experiments, ns). Statistical analysis was carried out using paired t-tests for each gene. (**E**) Schematic representation of TrkB isoforms analyzed. Top panel (i) shows the splicing isoforms of TrkB gene containing the N-terminus (NTRK2 e5/6). Full length TrkB and isoforms TrkB-T-Shc (NTRK2 e17/19) and TrkB-T1 (NTRK2 e15/16). Red arrows show the location of the primers utilized to amplify the specific isoforms. Bottom panel (ii) shows the full length TrkB proteins showing the corresponding protein domains to corresponding exons by color coding. Adapted from [62]. (**F**) Analysis of NTRK2 isoform expression by ddPCR in male cortical neurons under control or ASH1L knockdown conditions. Data was normalized to GAPDH and then normalized to control and is shown as counts/ng of DNA for three independent experiments.

Solid blue bars are control shRNA samples while hashed blue and white bars are ASH1L-shRNA samples for the following transcripts: *ASH1L* (Control-shRNA = 0.430 ± 0.088 *vs.* ASH1L-shRNA = 0.131 ± 0.010; ****P< 0.0001); *NTRK2* full length (control-shRNA = 0.371 ± 0.005 *vs.* ASH1L-shRNA = 0.170 ± 0.006; ****P < 0.0001); *NTRK2 e5/6* (control-shRNA = 0.499 ± 0.05 *vs.* ASH1L-shRNA=0.279 ± 0.013; ****P< 0.0001); *NTRK2 e15/16* (control-shRNA = 0.381 ± 0.010 *vs.* ASH1L-shRNA=0.175 ± 0.010; ****P< 0.0001); and *NTRK2 e17/19* (control-shRNA = 0.339 ± 0.027 *vs.* ASH1L-shRNA=0.495 ± 0.043; ****P < 0.0001).

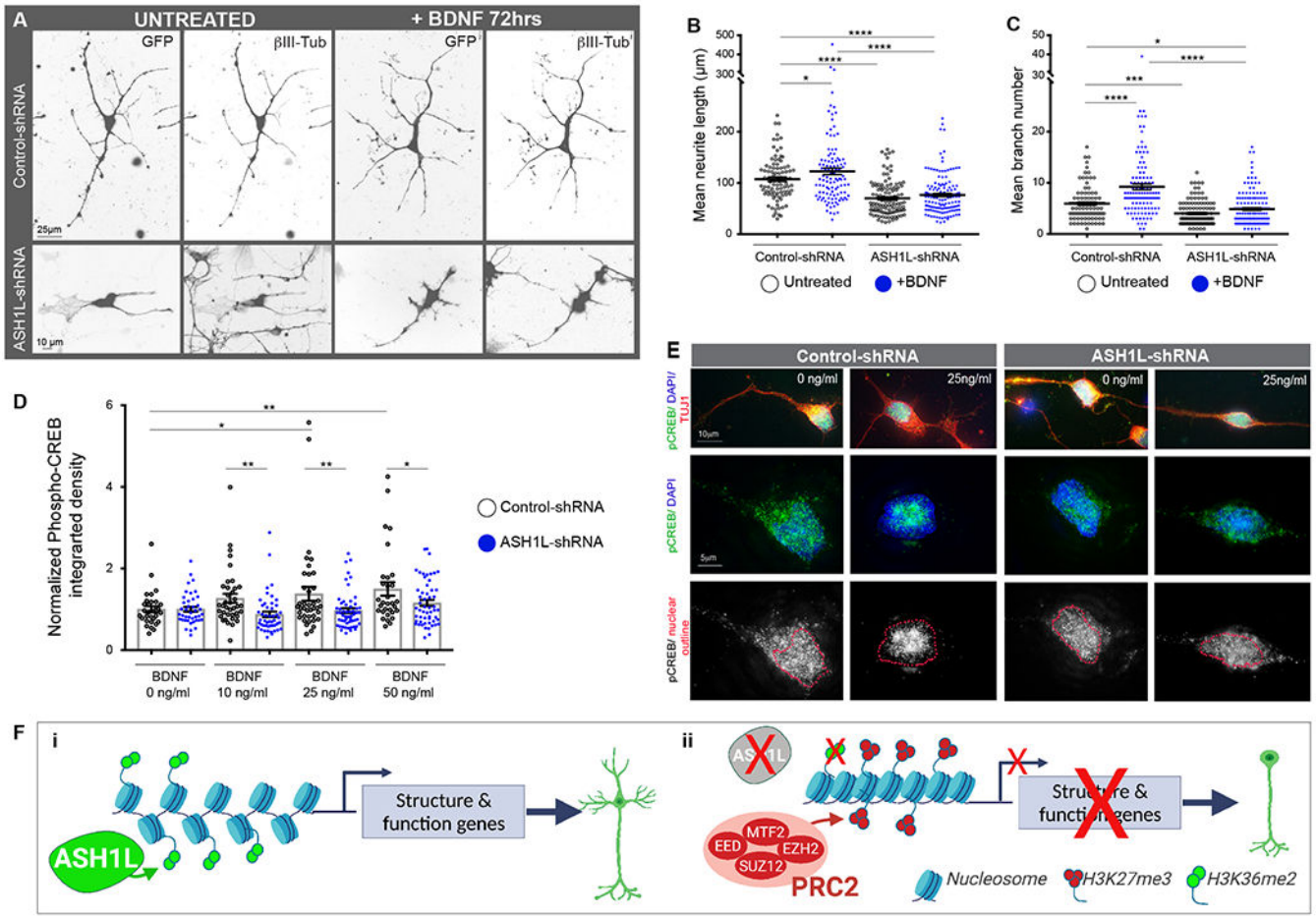

Figure 4. Loss of ASH1L reduces CREB activation by BDNF.

(**A**) Representative images are shown for neurons electroporated with GFP and either control shRNA or ASH1L shRNA constructs. Neurons treated with 0 or 10 ng/ml of BDNF for 3 days after puromycin selection positive for GFP and with β-III-Tubulin (β-III-Tub) shown. Neurons were analyzed at day 35 of neuronal induction. Scale bar, 25μm for controls and 10μm for ASH1L-shRNA samples. In general, neurons were nucleofected at day 29 and analyzed at day 35. For ease of viewing images were processed from RGB to luminescence in ImageJ and then inverted. (**B**) Mean neurite length in cortical neurons under control or ASH1L knockdown with or without 72hr BDNF treatment. Untreated samples are shown in open black circles and BDNF treated samples are shown in solid blue circles. Control shRNA = 107.3 ± 4.36, n = 93 cells; Control shRNA +BDNF = 122.7 ± 6.29, n = 111 cells; ASH1L-shRNA = 69.89 ± 3.179, n = 112 cells; and ASH1L-shRNA +BDNF= 76.46 ± 3.15, *n* = 144 cells. ****P < 0.0001, and * P < 0.02. If no p-values are shown that denotes that the differences were not significant. (**C**) Mean branch number is shown for cortical neurons under control or ASH1L-shRNA knockdown with or without 72hr BDNF treatment. Untreated samples are shown in open black circles and BDNF treated samples are shown in solid blue circles. Control shRNA = 5.93 ± 0.34; Control shRNA +BDNF = 9.22 ± 0.57; ASH1L-shRNA = 4.01 ± 0.23; and ASH1L-shRNA +BDNF = 4.86 ± 0.27. ***P < 0.0001, ***P < 0.0006, and * P <0.045. If no p-values are shown that denotes that the

differences were not significant. All measurements are shown per cell for each condition for four independent experiments. Mean is shown as the middle line and error bars are SEM. Statistical analysis was conducted using uncorrected Fisher's test for multiple comparisons with ordinary one-way ANOVA. **(D)** Activation of phospho–CREB is reduced in ASH1L knockdown neurons. Control or ASH1L shRNA transfected neurons were acutely exposed for 15 minutes to increasing doses of BDNF (0, 10, 25 and 50 ng/ml) to measure the nuclear translocation of phospho-CREB. Neurons were analyzed at day 34 of neuronal induction. Analysis of phospho-CREB nuclear levels was conducted by measuring integrated density on nuclear region of interest (ROI) after background subtraction in images acquired in a widefield fluorescent microscope. All values were normalized to the mean average value of the BDNF 0ng/ml samples for each experiment both in control-shRNA (open black circle) and ASH1L-shRNA (solid blue circle). Control-shRNA + 0ng/ml BDNF =1 ± 0.077, n=31 cells; *vs.* ASH1L-shRNA + 0ng/ml BDNF = 1 ± 0.060, n=41 cells. Control-shRNA +10ng/ml BDNF = 1.27 ± 0.111, n=38 cells; *vs.* ASH1L-shRNA + 10ng/ml BDNF = 0.87 ± 0.069, n=48 cells, ** $P < 0.006$. Control-shRNA +25ng/ml BDNF = 1.379 ± 0.171, n=39 cells; *vs.* ASH1L-shRNA + 25ng/ml BDNF = 0.9665 ± 0.060, n=55 cells, ** $P < 0.0025$. Control-shRNA +50ng/ml BDNF = 1.498 ± 0.166, n=31; *vs.* ASH1L-shRNA + 50ng/ml BDNF = 1.15 ± 0.074, n=55 cells, * $P < 0.02$. Control-shRNA + 0ng/ml BDNF *vs.* Control-shRNA +10ng/ml BDNF. Control-shRNA + 0ng/ml BDNF *vs.* Control-shRNA +25ng/ml BDNF, * $P < 0.02$. Control-shRNA + 0ng/ml BDNF *vs.* Control-shRNA +50ng/ml BDNF, ** $P < 0.003$. If no p-values are shown that denotes that the differences were not significant. All values are shown as mean ± SEM. All statistical analysis was carried out using uncorrected Fisher's test for multiple comparisons in one-way ANOVA on all data points for three independent experiments. (**E**) Super resolution microscopy confirms increased nuclear phospho-CREB signal in control neurons compared to ASH1L knockdown neurons in response to exogenous BDNF. Representative images are shown for neurons transfected with either control-shRNA or ASH1L-shRNA that were either untreated (0 ng/ml) or treated with BDNF (25ng/ml). Top panels show phospho-CREB (green) and TUJ1 (β-III-Tubulin) a pan-neuronal marker (red), in transfected neurons. Middle panels show co-immunostaining of phospho-CREB (green) and nuclear stain DAPI (blue). Bottom panels show the phospho-CREB signal in grey, and the nucleus is outlined in red. (**F**) Model depicting epigenetic regulation by ASH1L and PRC2 and their influence in neuronal morphogenesis. (i) ASH1L regulates genes that control neuronal structure and function by demethylating H3K36 (green) and preventing repression by PRC2, leading to normal morphogenesis. (ii) Reduction in ASH1L levels lead to reduce levels of H3K36me2 in genes that control neuronal structure and function allowing PRC2 to trimethylate H3K27 (red), leading to genes that contribute to neuronal morphogenesis leading to a reduction in neuronal arborization.